Aalto University

OPEN ACCESS

This is an electronic reprint of the original article.
This reprint may differ from the original in pagination and typographic detail.

Röntynen, J.; Ojanen, T.

Topological Superconductivity and High Chern Numbers in 2D Ferromagnetic Shiba Lattices

Published in:
Physical Review Letters

DOI:
10.1103/PhysRevLett.114.236803

Published: 01/01/2015

Document Version
Publisher's PDF, also known as Version of record

Please cite the original version:
Röntynen, J., & Ojanen, T. (2015). Topological Superconductivity and High Chern Numbers in 2D Ferromagnetic Shiba Lattices. *Physical Review Letters*, *114*(23), 1-5. Article 236803.
https://doi.org/10.1103/PhysRevLett.114.236803

This material is protected by copyright and other intellectual property rights, and duplication or sale of all or part of any of the repository collections is not permitted, except that material may be duplicated by you for your research use or educational purposes in electronic or print form. You must obtain permission for any other use. Electronic or print copies may not be offered, whether for sale or otherwise to anyone who is not an authorised user.

Topological Superconductivity and High Chern Numbers in 2D Ferromagnetic Shiba Lattices

Joel Röntynen and Teemu Ojanen*
O. V. Lounasmaa Laboratory (LTL), Aalto University, P. O. Box 15100, FI-00076 AALTO, Finland
(Received 18 December 2014; published 12 June 2015)

Inspired by the recent experimental observation of topological superconductivity in ferromagnetic chains, we consider a dilute 2D lattice of magnetic atoms deposited on top of a superconducting surface with a Rashba spin-orbit coupling. We show that the studied system supports a generalization of $p_x + ip_y$ superconductivity and that its topological phase diagram contains Chern numbers higher than $\xi/a(\gg 1)$, where ξ is the superconducting coherence length and a is the distance between the magnetic atoms. The signatures of nontrivial topology can be observed by STM spectroscopy in finite-size islands.

DOI: 10.1103/PhysRevLett.114.236803 PACS numbers: 74.50.+r, 73.63.Nm, 74.78.Na, 74.78.Fk

Introduction.—The recent experiment reporting signatures of topological superconductivity in magnetic chains, consisting of arrays of magnetic atoms on top of a superconductor, has opened up a remarkable chapter in the pursuit of novel topological phases of matter [1]. Promising signatures of topological superconductivity and Majorana bound states have previously been reported in nanowire setups [2–5], although the later analysis of the zero-bias peak attributed to Majorana states has revealed a number of alternative explanations. The groundbreaking experiment in magnetic chains directly demonstrated that the midgap states are localized at the ends of the chain, corroborating the topological character of these states. These developments are important since realization of topological superconductivity in 1D networks [6,7] would open up a route towards topological quantum computation [8].

Motivated by the recent experiment and anticipating future developments, we consider a 2D lattice of ferromagnetic magnetic moments on a 2D superconducting surface with a Rashba spin-orbit coupling. Magnetic moments bind Yu-Shiba-Rusinov subgap states [9–13] with wave functions decaying as $e^{-r/\xi}/r^{1/2}$. Therefore the Shiba states have strong overlap with a large number of neighboring sites when $a < \xi$, where ξ is the superconducting coherence length and a is the lattice constant of the magnetic atoms. In the regime where the direct overlap of the orbitals of the magnetic atoms is negligible, the hybridization of the Shiba states still enable a subgap band formation. Following the treatments in Refs. [14–16], we derive an effective long-range 2D hopping model and study its topological properties in the deep-dilute impurity regime. The characteristic energy scales of the system are the isolated Shiba energy ϵ_0 and the hybridization energy $\Delta/(k_F a)^{1/2}$ of two impurities. We study the topological phase diagram as a function of these parameters by evaluating Chern numbers classifying the phases. In the physically relevant circumstances the distance between adjacent magnetic moments satisfies $\xi/a \sim 10 - 10^3$, so the effective Hamiltonian describing the Shiba lattice includes long hoppings between $\mathcal{O}(\xi/a)$ nearest neighbors before the exponential suppression cuts them off. The detailed properties of the 1D long-range Shiba models [14–21] are known to have important differences compared to the short-range toy models [22–25]. We show that the competition between a large number of long-range hopping terms gives rise to a complicated Chern number hierarchy. The studied system generally supports phases with high Chern numbers of the order of ξ/a which leads to a significantly richer phase diagram compared to short-range toy models [26]. Nonvanishing Chern numbers indicate the existence of gapless edge states that could be probed in STM experiments. We will show that the local density of states (LDOS) in finite-size systems exhibits signatures of the edge states, providing smoking-gun evidence of the bulk topological order.

Model of ferromagnetic Shiba lattices.—We begin by outlining the derivation of a low-energy model describing the subgap spectrum of a 2D s-wave superconductor with an array of magnetic impurities arranged in a 2D lattice such as the one in Fig 1. The model is valid for general 2D lattice geometries, though later we consider a square lattice. The derivation proceeds similarly to the one presented in Ref. [14] for a helical Shiba chain and that of the 1D

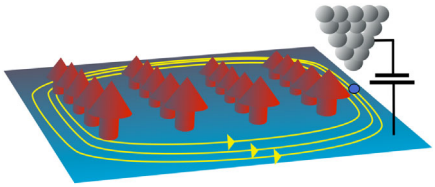

FIG. 1 (color online). Array of magnetic impurities on an s-wave superconductor form a 2D Shiba lattice. This system supports a generalized $p_x + ip_y$ superconductivity with high Chern numbers. The subgap density of states due to the gapless edge states can be probed by STM spectroscopy.

 © 2015 American Physical Society

ferromagnetic chain in Ref. [16]. Therefore the details are relegated to the Supplement Material [27].

The Bogoliubov–de Gennes (BdG) Hamiltonian describing the system is $\mathcal{H} = \mathcal{H}^{(\mathrm{bulk})} + \mathcal{H}^{(\mathrm{imp})}$, consisting of two parts

$$\mathcal{H}^{(\mathrm{bulk})} = \tau_z[\xi_{\mathbf{k}} + \alpha_R(k_y\sigma_x - k_x\sigma_y)] + \Delta\tau_x,$$
$$\mathcal{H}^{(\mathrm{imp})} = -J\sum_j \mathbf{S}_j \cdot \boldsymbol{\sigma}\delta(\mathbf{r} - \mathbf{r}_j), \quad (1)$$

where $\mathcal{H}^{(\mathrm{bulk})}$ describes bulk electrons in a 2D system and $\mathcal{H}^{(\mathrm{imp})}$ represents the contribution of the magnetic atoms forming a lattice. These expressions have been written in the Nambu spinor basis $\hat{\Psi} = (\hat{\psi}_\uparrow, \hat{\psi}_\downarrow, \hat{\psi}_\downarrow^\dagger, -\hat{\psi}_\uparrow^\dagger)^T$ and the Pauli matrices $\boldsymbol{\tau}$ and $\boldsymbol{\sigma}$ describe the particle-hole and the spin degree of freedom. In the above equations $\xi_{\mathbf{k}}$ is the kinetic energy, α_R is the Rashba spin-orbit coupling, and Δ is the superconducting pairing in the substrate. In the absence of superconductivity the 2D bulk has two Rashba-split Fermi surfaces with distinct Fermi momenta $k_F^\pm = k_F(\sqrt{1+\lambda^2} \mp \lambda)$ and the densities of states at the Fermi level $\mathcal{N}_\pm = \mathcal{N}[1 \mp \lambda/\sqrt{1+\lambda^2}]$. Here we have defined a dimensionless spin-orbit strength $\lambda = \alpha_R/(\hbar v_F)$, the density of states $\mathcal{N}$, and the Fermi velocity v_F in the absence of the Rashba coupling. Magnetic atoms, located at positions $\mathbf{r}_j$, are characterized by their spin $\boldsymbol{S}_j$ and coupling to the bulk electrons with the exchange coupling J. Motivated by Ref. [1], we concentrate on the ferromagnetic ordering where all $\boldsymbol{S}_j$ are perpendicular to the surface. After a number of steps outlined in the Supplemental Material [27], the BdG eigenvalue problem $\mathcal{H}\Psi = E\Psi$ leads to the relation

$$[\boldsymbol{S}_i \cdot \sigma - J_E(0)]\Psi(\mathbf{r}_i) = -\sum_{j\neq i} J_E(\mathbf{r}_i - \mathbf{r}_j)\Psi(\mathbf{r}_j), \quad (2)$$

where $J_E(\mathbf{r}) = JS\int \frac{d\mathbf{k}}{(2\pi)^2} e^{i\mathbf{k}\cdot\mathbf{r}}[E - \mathcal{H}_{\mathbf{k}}^{(\mathrm{bulk})}]^{-1}$ and $S = |\boldsymbol{S}_j|$. Relation Eq. (2) provides a closed set of equations for the spinor at the impurity positions.

Because of the doubling of the degrees of freedom in the BdG formulation, a single magnetic atom will give rise to two subgap bound states with energies $\pm\varepsilon_0 = \pm\Delta[(1-\alpha^2)/(1+\alpha^2)]$ where $\alpha = \pi\mathcal{N}JS$ is the dimensionless impurity strength. As discussed in Refs. [14,16,20], for a deep-dilute impurity arrangement satisfying $\alpha \approx 1$ and $[1/(k_F a)^{1/2}] \ll 1$ we can accurately study the Shiba bands in the two-component basis $\Psi_j'(\mathbf{r}_j) \equiv \Psi_j' = (u(\mathbf{r}_j)v(\mathbf{r}_j))^T$ of decoupled impurity states at site $\mathbf{r}_j$. Here $u(\mathbf{r}_j)$ and $v(\mathbf{r}_j)$ are the eigenstates to the single-impurity problem with energies $\varepsilon_0 \approx \Delta(1-\alpha)$ and $-\varepsilon_0$.

Projecting Eq. (2) to the two basis states we obtain a reduced problem $H\Psi' = E\Psi'$ where

$$H_{ij} = \begin{pmatrix} h_{ij} & \Delta_{ij} \\ (\Delta_{ij})^\dagger & -h_{ij} \end{pmatrix}. \quad (3)$$

The effective BdG Hamiltonian, Eq. (3), is determined by the matrices

$$h_{ij} = \begin{cases} \varepsilon_0 & i = j \\ -\frac{\Delta^2}{2}[\tilde{I}_1^-(r_{ij}) + \tilde{I}_1^+(r_{ij})] & i \neq j \end{cases},$$
$$\Delta_{ij} = \begin{cases} 0 & i = j \\ \frac{\Delta}{2}[\tilde{I}_0^+(r_{ij}) - \tilde{I}_0^-(r_{ij})]\frac{x_{ij}-iy_{ij}}{r_{ij}} & i \neq j \end{cases}.$$

In the above expression $r_{ij} = |\mathbf{r}_i - \mathbf{r}_j|$, and x_{ij} and y_{ij} are components of $\mathbf{r}_i - \mathbf{r}_j \equiv (x_{ij}, y_{ij})$. The hopping elements are expressed in terms of the functions

$$\tilde{I}_0^\pm(r) = \frac{\mathcal{N}_\pm}{\mathcal{N}}\Re[iJ_1(k_F^\pm r + ir/\xi) + H_{-1}(k_F^\pm r + ir/\xi)],$$
$$\tilde{I}_1^\pm(r) = \frac{\mathcal{N}_\pm}{\mathcal{N}}\frac{1}{\Delta}\Re[J_0(k_F^\pm r + ir/\xi) + iH_0(k_F^\pm r + ir/\xi)],$$

where J_n and H_n denote the Bessel and Struve functions of order n, $\xi = [(v_F\sqrt{1+\lambda^2})/\Delta]$ is the Rashba modified coherence length and $\Re$ stands for the real part of the expression on its right side. The effective model Eq. (3) is valid for deep-lying energy states $E \ll \Delta$, with corrections proportional to $(E/\Delta)^2$.

The key ingredients of the low-energy description [Eq. (3)] are the coexistence of superconductivity, ferromagnetic ordering, and the Rashba coupling, all of which have been demonstrated in the recent experiment [1]. To appreciate the crucial role of the spin-orbit coupling we note that Δ_{ij} vanishes when $\alpha_R = 0$. The pairing function has the form $\Delta_{ij} = \Delta(x_{ij} - iy_{ij})f(r_{ij})$, where $f(r_{ij}) = [\tilde{I}_0^+(r_{ij}) - \tilde{I}_0^-(r_{ij})]/2$. This indicates that the low-energy description [Eq. (3)] has an odd-pairing symmetry $\Delta_{ij} = -\Delta_{ji}$ that generalizes the $p_x + ip_y$-type pairing. An ordinary chiral p-wave pairing would result if $f(r_{ij})$ was nonvanishing only for the nearest-neighbor hopping on a square lattice. However, in the model Eq. (3) the normal hopping and the pairing function decay as $f(r) \propto (e^{-r/\xi}/r^{1/2})$ [27], so in the physically relevant case $\xi/a \sim 10 - 10^3$ the model includes non-negligible hopping between dozens or hundreds of nearest neighbors. The relation between the model Eq. (3) and a 2D chiral p-wave superconductor is similar to the relation between the long-range 1D Shiba models and Kitaev's toy model [28]. Since a chiral p-wave pairing is the prototype of 2D topological superconductivity, it is natural to expect that the model Eq. (3) also supports topologically nontrivial phases. Below we will discuss how the long-range hopping has a dramatic impact on the topological properties and leads to remarkably complex phase diagrams.

Topological properties.—Topological properties of the model Eq. (3) on a square lattice are conveniently studied in momentum space. Defining Fourier transforms

$$d_x(\mathbf{k}) = \Re \sum_j \Delta_{ij} e^{ik_x x_{ij} + ik_y y_{ij}},$$
$$d_y(\mathbf{k}) = \Im \sum_j \Delta_{ij} e^{ik_x x_{ij} + ik_y y_{ij}},$$
$$d_z(\mathbf{k}) = \sum_j h_{ij} e^{ik_x x_{ij} + ik_y y_{ij}},$$

the Hamiltonian in momentum space is expressed as $H(\mathbf{k}) = \mathbf{d}(\mathbf{k}) \cdot \boldsymbol{\sigma}$ with energies $E(k) = \pm|\mathbf{d}|$. The components of $\mathbf{d} = (d_x, d_y, d_z)$ do not allow a representation in terms of the elementary functions. The topological phase diagram of the studied model, which belongs to the Altland-Zirnbauer symmetry class D [29], is revealed by evaluating the Chern number

$$C = \frac{1}{4\pi} \int_{\mathrm{BZ}} d^2\mathbf{k} \frac{\mathbf{d} \cdot \partial_{k_x}\mathbf{d} \times \partial_{k_y}\mathbf{d}}{|\mathbf{d}|^3}, \tag{4}$$

where the integration is performed over the Brillouin zone $k_x, k_y \in [-(\pi/a), (\pi/a)]$. The Chern number takes integer values and describes how many times the vector $\hat{\mathbf{d}} = \mathbf{d}/|\mathbf{d}|$ wraps around the unit sphere. Below we compute Chern numbers as a function of the relevant parameters ε_0 and $k_F a$. The bulk-boundary correspondence implies that topological states with Chern number $C = q$ support $|q|$ branches of chiral gapless modes localized near the edge. The sign of C determines the chirality of the edge modes. In nonsuperconducting systems C determines a quantized Hall conductance whereas in superconducting systems only the thermal Hall conductance is quantized and the edge states are propagating Majorana modes [30].

To understand qualitative features of the phase diagram, it is important to consider the connection between the long-range hopping and the Chern number. Intuitively this can be understood by noting that the nth hopping in x and y direction gives rise to such terms in d_i as $\cos(nk_{x/y}a), \sin(nk_{x/y}a)$ that oscillate more rapidly with increasing n. Thus, the number of times $\hat{\mathbf{d}}$ may cover the unit sphere will generally increase with n. Employing the asymptotic approximations for the Bessel and Struve function [27], one can see that the nth hopping terms decay as $[|\Delta|/(k_F a)^{1/2}](e^{-an/\xi}/n^{1/2})$, so the decay is very slow for the hopping range $n < \xi/a$. In addition to the monotonic decay, the nth hopping terms oscillate rapidly with wave vectors $nk_F^{\pm}a$ so the phase diagram results from an effective competition of roughly $\mathcal{O}(\xi/a)$ different hopping terms. In a recent study of toy models of two-band Chern insulators it was discussed how models with hopping range n may give rise to Chern numbers scaling between n and n^2 depending on the details of the model

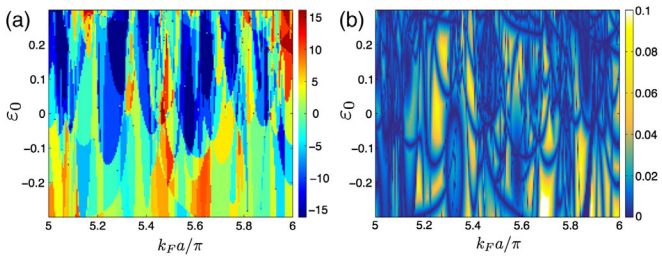

FIG. 2 (color online). (a) Chern number phase diagram for $\xi/a = 10$ and $\lambda = 0.05$. (b) Minimum of the positive energy branch $\min_k E(k)$ in units of Δ for the same parameters. Different phases are separated by an energy gap closing.

[31]. Remarkably, the model Eq. (3) provides a concrete physical realization of a topological superconductor where Chern numbers are of the order of or larger than the effective hopping range ξ/a, as in the toy insulator models studied in Ref. [31].

In Figs. 2 and 3 we have plotted topological phase diagrams as a function of the single-impurity energy ε_0 and parameter $k_F a$ controlling the hybridization of the impurity states. Different Chern numbers classify different phases that are separated by a closing of the energy gap determined by the condition $\min_k E(k) = 0$. One can clearly see that for spin-orbit strength $\lambda = 0.05$ corresponding to a momentum splitting $|k_F^{\pm} - k_F| = 0.05k_F$ give rise to a large number of different phases with high Chern numbers and topological energy gaps $E_{\mathrm{gap}} = 2\min_k E(k)$ of the order of 0.1Δ. These energies are still within the validity regime of the low-energy description, Eq. (3). The number of different topological phases and the highest Chern numbers having non-negligible occurrence are of the order of ξ/a. In Fig. 4 we plot the spectrum of Eq. (3) calculated in a strip geometry. Diagonalization in a semi-infinite system reveals the existence of the edge states dictated by the bulk-boundary correspondence.

Observable consequences and discussion.—Chern numbers classify different topological states and determine the number of edge modes. The topological edge modes support a quantized thermal conductance $G_T = |C| \times G_0$ along the propagation direction, where $G_0 = (\pi^2 k_B^2 T/3h)$.

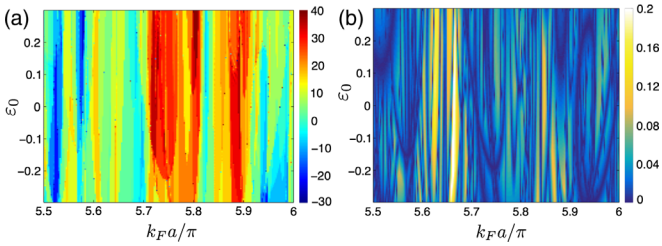

FIG. 3 (color online). (a) Chern number phase diagram for $\xi/a = 30$ and $\lambda = 0.05$. (b) Minimum of the positive energy branch $\min_k E(k)$ in units of Δ for the same parameters used in (a).

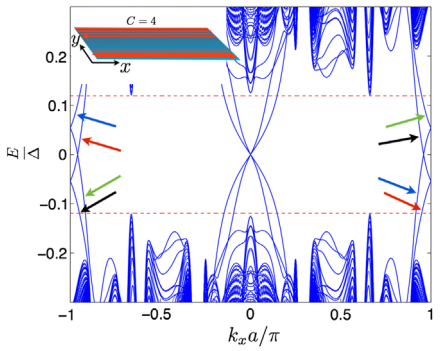

FIG. 4 (color online). Spectrum of an infinite strip as a function of momentum k_x corresponding to Chern number $C = 4$. Both edges support four chiral edge modes traversing the gap. Because of the periodicity of the Brillouin zone, the edge states close to $k_x = -\pi/a$ and $k_x = \pi/a$ describe the same set of states as indicated by the arrows. The dotted line marks the gap edge calculated for an infinite system. The figure corresponds to the case $\xi/a = 10$, $\varepsilon_0/\Delta = -0.25$, $k_F a/\pi = 3.56$, $\lambda = 0.05$ and the length in the y direction is $L_y = 200a$.

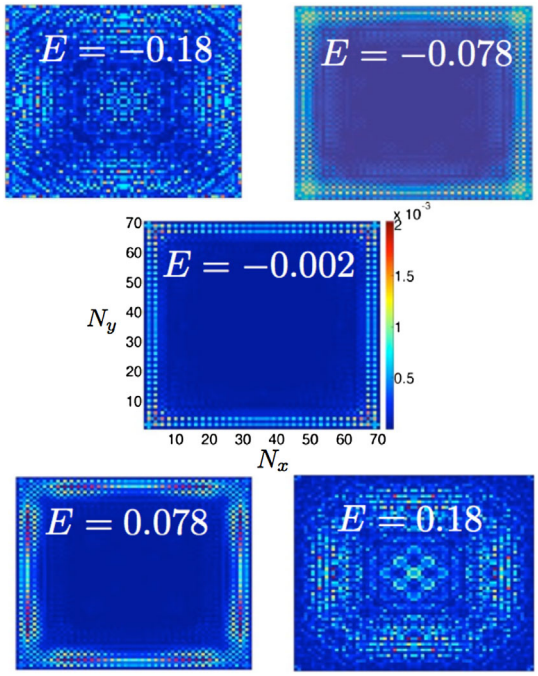

FIG. 5 (color online). Local density of states in a finite 70×70 lattice (in arbitrary units) corresponding to a bulk state with $C = 3$. All the energies are in the units of Δ and correspond to tunneling voltages $V = E/e$. Near the center of the gap the LDOS is suppressed in the bulk but enhanced on the edges due to the topological edge states. The figure corresponds to the case $\xi/a = 10$, $\varepsilon_0/\Delta = -0.22$, $k_F a/\pi = 4.9$, $\lambda = 0.05$.

While this provides a method to distinguish different phases such measurement requires high accuracy and is challenging at the moment. A great advantage of Shiba systems is that they can be probed locally by STM spectroscopy. Signatures of Majorana wave functions localized at the ends of magnetic chains were recently observed. Analogously, the signatures of 2D topological order could be detected through STM spectroscopy where the edge states could be observed in the LDOS of finite Shiba arrays as indicated in Fig. 1.

Diagonalization [Eq. (3)] in a finite square lattice enables us to evaluate the LDOS defined by $N(\mathbf{r}, E) = \sum_n |u_n(\mathbf{r})|^2 \delta(E - E_n) + |v_n(\mathbf{r})|^2 \delta(E + E_n)$. Here $u_n(\mathbf{r})$ and $v_n(\mathbf{r})$ are the particle and hole components of the eigenstate with energy E_n. In the absence of magnetic atoms the system is in the trivial state and $N(\mathbf{r}, E) = 0$ for $|E| < \Delta$. However, the topological edge modes of finite Shiba lattices with $C \neq 0$ show up in the subgap LDOS. Away from the phase boundaries the bulk spectrum is always gapped, while the edge states traverse the gap. Therefore, the LDOS near the center of the gap $E/\Delta \ll 1$ should reveal the existence of topological edge states. Furthermore, since the edge states are localized at the sample edge we expect that the midgap LDOS $N(\mathbf{r}, E)$ is peaked when the coordinate $\mathbf{r}$ is located near the boundary and suppressed in the bulk. As illustrated in Fig. 5, even relatively small systems exhibit these important features. STM spectroscopy is not sensitive to the precise value of the Chern number of the state but can detect nonzero values through the subgap LDOS. The fact that the low-lying excitations are localized in the vicinity of the edges provides strong evidence of the bulk topological order in the system. As discussed in the Supplemental Material [27], weak disorder does not destroy the physical picture. It is also possible to extract qualitative information about different topological states through the LDOS [27].

As discussed in Ref. [1], the next challenges after the confirmation of the topological superconductivity in 1D ferromagnetic chains include studies of topological properties of 2D islands observed in the experimental setup. In the experiment iron atoms are densely packed a few Å apart so that the atomic d orbitals overlap directly and give rise to the ferromagnetic ordering. Our theory addresses the situation where the distance between magnetic moments is of the order of nanometers and the direct overlap of atoms is negligible. In this case the ferromagnetic ordering may be obtained due to the interplay of Ruderman-Kittel-Kasuya-Yosida coupling, Rashba coupling, and crystal field splitting [18]. The key ingredients leading to the rich topological properties discovered in our work are the coexistence of superconductivity, the ferromagnetic ordering of adatoms, and the Rashba coupling on the surface, all of which are confirmed in Ref. [1]. As discussed above, the energy gaps for various Chern number phases can reach a few multiples of 0.1Δ corresponding to temperatures of the order of 1 K. Considering that Pb surfaces may give rise to a spin-orbit coupling comparable to the one assumed in our calculations and that STM signatures of the edge modes are observable already in small systems, chances of finding 2D topological superconductivity in ferromagnetic islands seem very promising.

Summary and outlook.—Motivated by the recent experimental discovery of topological superconductivity in ferromagnetic chains, we studied a 2D ferromagnetic Shiba lattices. We reported that these systems support a generalized $p_x + ip_y$ superconductivity with a large number of phases and Chern numbers higher than $\xi/a \gg 1$ where ξ is the superconducting coherence length and a is the Shiba lattice constant. As in the 1D case, the signatures of topological edge states can be observed by STM spectroscopy. A more systematic exploration of phase diagrams, the topological properties of different lattice geometries and lattice imperfections, and exploration of different scenarios to tune the topological properties are left for future studies.

The authors acknowledge Alex Weststrom and Kim Pöyhönen for illuminating discussions, the computational resources provided by Aalto Science-IT project, and the Academy of Finland for support.

*Corresponding author.
teemuo@boojum.hut.fi

[1] S. Nadj-Perge, I. K. Drozdov, J. Li, H. Chen, S. Jeon, J. Seo, A. H. MacDonald, B. Andrei Bernevig, and A. Yazdani, Science **346**, 602 (2014).
[2] R. M. Lutchyn, J. D. Sau, and S. Das Sarma, Phys. Rev. Lett. **105**, 077001 (2010).
[3] Y. Oreg, G. Refael, and F. von Oppen, Phys. Rev. Lett. **105**, 177002 (2010).
[4] V. Mourik, K. Zuo, S. M. Frolov, S. R. Plissard, E. P. A. M. Bakkers, and L. P. Kouwenhoven, Science **336**, 1003 (2012).
[5] A. Das, Y. Ronen, Y. Most, Y. Oreg, M. Heiblum, and H. Shtrikman, Nat. Phys. **8**, 887 (2012).
[6] J. Alicea, Y. Oreg, G. Refael, F. von Oppen, and M. P. A. Fisher, Nat. Phys. **7**, 412 (2011).
[7] J. Li, T. Neupert, B. A. Bernevig, and A. Yazdani, arXiv:1404.4058.
[8] C. Nayak, S. H. Simon, A. Stern, M. Freedman, and S. Das Sarma, Rev. Mod. Phys. **80**, 1083 (2008).
[9] L. Yu, Acta Phys. Sin. **21**, 75 (1965).
[10] H. Shiba, Prog. Theor. Phys. **40**, 435 (1968).
[11] A. I. Rusinov, JETP Lett. **9**, 85 (1969).
[12] M. I. Salkola, A. V. Balatsky, and J. R. Schrieffer, Phys. Rev. B **55**, 12648 (1997).
[13] A. Yazdani, B. A. Jones, C. P. Lutz, M. F. Crommie, and D. M. Eigler, Science **275**, 1767 (1997).
[14] F. Pientka, L. I. Glazman, and F. von Oppen, Phys. Rev. B **88**, 155420 (2013).
[15] F. Pientka, L. I. Glazman, and F. von Oppen, Phys. Rev. B **89**, 180505 (2014).
[16] P. M. R. Brydon, H.-Y. Hui, and J. D. Sau, Phys. Rev. B **91**, 064505 (2015).
[17] A. Heimes, P. Kotetes, and G. Schön, Phys. Rev. B **90**, 060507(R) (2014).
[18] A. Heimes, D. Mendler, and P. Kotetes, New J. Phys. **17**, 023051 (2015).
[19] J. Röntynen and T. Ojanen, Phys. Rev. B **90**, 180503 (2014).
[20] A. Weststrom, K. Pöyhönen, and T. Ojanen, Phys. Rev. B **91**, 064502 (2015).
[21] I. Reis, D. J. J. Marchand, and M. Franz, Phys. Rev. B **90**, 085124 (2014).
[22] T. P. Choy, J. M. Edge, A. R. Akhmerov, and C. W. J. Beenakker, Phys. Rev. B **84**, 195442 (2011).
[23] S. Nadj-Perge, I. K. Drozdov, B. A. Bernevig, and A. Yazdani, Phys. Rev. B **88**, 020407(R) (2013).
[24] M. M. Vazifeh and M. Franz, Phys. Rev. Lett. **111**, 206802 (2013).
[25] K. Pöyhönen, A. Weststrom, J. Röntynen, and T. Ojanen, Phys. Rev. B **89**, 115109 (2014).
[26] S. Nakosai, Y. Tanaka, and N. Nagaosa, Phys. Rev. B **88**, 180503 (2013).
[27] See Supplemental Material at http://link.aps.org/supplemental/10.1103/PhysRevLett.114.236803 for details.
[28] A. Y. Kitaev, Phys. Usp. **44**, 131 (2001).
[29] A. P. Schnyder, S. Ryu, A. Furusaki, and A. W. W. Ludwig, Phys. Rev. B **78**, 195125 (2008); S. Ryu, A. P. Schnyder, A. Furusaki, and A. W. W. Ludwig, New J. Phys. **12**, 065010 (2010).
[30] G. E. Volovik, *The Universe in a Helium Droplet* (Oxford University Press, New York, 2003).
[31] M. Udagawa and E. J. Bergholtz, J. Stat. Mech. (2014) P10012.